Journal of The Electrochemical Society

The Electrochemical Society
Advancing solid state & electrochemical science & technology

OPEN ACCESS

Overcharge Study in $Li_4Ti_5O_{12}$ Based Lithium-Ion Pouch Cell

To cite this article: Arnaud Devie *et al* 2016 *J. Electrochem. Soc.* **163** A2611

View the article online for updates and enhancements.

You may also like

- Novel Method for Using Force in Incremental Capacity Analysis for Capacity Fading Estimation
Nassim Abdul Samad, Youngki Kim, Jason B Siegel et al.
- Soh Indicator of EV Lithium-Ion Cell Based on Incremental Capacity
Akram Eddahech and Arnaud Delaille
- Degradation Analysis of Commercial Lithium-Ion Battery in Long-Term Storage
Taolin Lu, Ying Luo, Yixiao Zhang et al.

Your Lab in a Box!
The PAT-Tester-i-16: All you need for Battery Material Testing.
All-in-One Solution with integrated Temperature Chamber!
Cableless Connection for Battery Test Cells!
Fully featured Multichannel Potentiostat / Galvanostat / EIS!
www.el-cell.com +49 40 79012-734 sales@el-cell.com
EL-CELL®
electrochemical test equipment

This content was downloaded from IP address 3.145.50.83 on 25/04/2024 at 03:14

Overcharge Study in $Li_4Ti_5O_{12}$ Based Lithium-Ion Pouch Cell

II. Experimental Investigation of the Degradation Mechanism

Arnaud Devie,[a,*] Matthieu Dubarry,[a,,z] Hung-Ping Wu,[b] Tsung-Han Wu,[b] and Bor Yann Liaw[a,***]**

[a]*Electrochemical Power Systems Laboratory, Hawaii Natural Energy Institute, School of Ocean and Earth Science and Technology, University of Hawaii at Manoa, Honolulu, Hawaii 96822, USA*
[b]*Underwriters Laboratories Taiwan Co., Ltd., Peitou, Taipei City 112, Taiwan*

An $Li_4Ti_5O_{12}$ || $LiNi_{1/3}Mn_{1/3}Co_{1/3}O_2$ lithium-ion pouch cell has been subjected to an overcharge early in its cycle-life and kept cycling it up to 1500 cycles afterwards. We report on the non-invasive experimental verifications we conducted to corroborate our initial findings obtained via incremental capacity analysis. First, we used incremental capacity analysis on the negative electrode during overcharge to bring evidence of electrolyte reduction below 1 V vs. Li/Li^+. Second, we used X-ray computerized tomography (CT scan) to demonstrate that gas bubbles were trapped between layers of positive and negative electrodes, thereby disabling the ionic conduction pathway between the two and causing capacity fade. Third, we administered a massage to the pouch cell to establish that the gas bubbles could be displaced, thereby recovering about 60% of the faded capacity. Finally, we proposed a new approach based on the study of the open-circuit voltage to describe quantitatively the gains of active materials that led to the partial capacity recovery.

© The Author(s) 2016. Published by ECS. This is an open access article distributed under the terms of the Creative Commons Attribution 4.0 License (CC BY, http://creativecommons.org/licenses/by/4.0/), which permits unrestricted reuse of the work in any medium, provided the original work is properly cited. [DOI: 10.1149/2.0491613jes] All rights reserved.

Manuscript submitted August 8, 2016; revised manuscript received September 8, 2016. Published September 22, 2016.

Lithium-ion batteries remain as the choice for electric vehicles and utility-scale energy storage applications. The battery pack used in these applications usually comprises tens or hundreds of cells in series to reach a practical voltage of 300 to 600 V. Typically, the same charging or discharging current flows through a string at all time, which means that all cells in series typically charge or discharge at the same pace. A problem arises when one or more cells in the series that have less capacity than the others may get overcharged. In this study, we investigated the abuse tolerance of a lithium-ion cell under an overcharge scenario.

In part one of this work, we reported on a case study of an overcharging event that occurred after 125 cycles of aging $Li_4Ti_5O_{12}$ (LTO) || $LiNi_{1/3}Mn_{1/3}Co_{1/3}O_2$ (NMC) commercial cells used in energy storage systems.[1] Figure 1 summarizes the results of the long term cycling experiment as reported previously.[1] Apart from the controlled overcharge, the reference and overcharged (O/C) cells had been cycled under identical voltage, current and temperature conditions. While the reference cell exhibited an extremely small capacity fade over the course of 700 cycles, the overcharged cell lost about 23% of its initial capacity after 700 cycles (15% shortly after overcharge and an additional 8% from the 150th cycle to the 700th cycle).

In recent years, our battery research group has developed capabilities in emulating the degradation of lithium-ion cells for battery diagnosis and prognosis based on the application of incremental capacity analysis at the full cell level.[2–5] According to the results of this incremental capacity analysis, the overcharge imposed to the cell was found to introduce a two-stage degradation pattern. During the first stage, in the immediate aftermath the overcharge, a combination of 8% loss of lithium inventory (LLI), 15% of loss of active material on the delithiated positive electrode (LAM_{dePE}), and 15% loss of active material on the lithiated negative electrode (LAM_{liNE}) have been found to be responsible for the observed 15% capacity fade. In the second stage, which encompasses 600 cycles following the overcharge, we have found that an additional capacity fade, on the order of 8%, could be attributed to 8% LAM_{PE} and 8% LAM_{NE}.

Based on these findings, the hypothesis that gas evolution occurred at the electrodes induced by transient highly reductive conditions during the overcharge was developed. This hypothesis is described in details in the first part of this study[1] and summarized in the next section. In this follow up study, we investigated this hypothesis using X-ray computerized tomography (CT scan), a non-invasive, in-situ imaging investigation technique. First, we attempted to validate the assumption that highly reductive conditions were present at the time of the overcharge. Second, we attempted to visualize the existence of gas bubbles within the electrode stack. Finally, we attempted to displace these gas bubbles by hand massage in hope of restoring ionic conduction pathways to the supposedly deactivated portions of electrodes. If our hypothesis held and gas bubbles were indeed the main driver for capacity fade of the O/C cell, then one would expect to recover a large extent of the 23% of capacity lost following the overcharge.

Proposed overcharge degradation mechanism hypothesis.—Regarding the first stage (i.e. the overcharge itself); the occurrence of LLI suggests that electrolyte decomposition has been induced by localized severe reductive conditions likely to occur at the negative electrode, and/or localized severe oxidative conditions, which may occur at the positive electrode. Since gas evolution inside the cell has been shown to accompany LLI,[6–9] it is reasonable to assume that 8% LLI must translate into a very significant release of gas within the cell over a very short time frame. Such a rapid gas evolution might generate enough mechanical stress on the electrode stack to create mechanical separation (space) in between some portions of NE and PE and/or displacement of liquid electrolyte by gas bubbles, resulting in a blockage to the ionic pathway. Such a scenario would result in physical insulation of active material (AM) from both PE and NE in similar proportions, as suggested by an equal amount of LAM at the PE and NE in opposite lithiation states (i.e. 15% LAM_{dePE} and 15% LAM_{liNE}). A schematic of this mechanism is shown in Figure 1a. Insets (a-d) in Figure 1 depict a simplified schematic of an O/C LTO || NMC pouch cell, where a single layer of electrode stack is shown in a sealed soft pouch. The presence of liquid electrolyte is symbolized by a blue tint while gaseous products are pictured as white clouds. Initially, there is no trace of gas in the layers (Fig. 1a). During the overcharge event, gas was released as a product of electrolyte decomposition at the electrolyte || LTO interface (Fig. 1b) and produced tiny gas bubbles. These bubbles would then permeate toward the center of the pouch cell since it is the location that exhibits the least amount of resistance to any mechanical deformation (whereas corners and sides shall have high resistance to deformation). Once overcharge conditions were terminated, a finite volume of gas could gather and form a

*Electrochemical Society Student Member.
**Electrochemical Society Member.
***Electrochemical Society Fellow.
[z]E-mail: matthieu@hawaii.edu

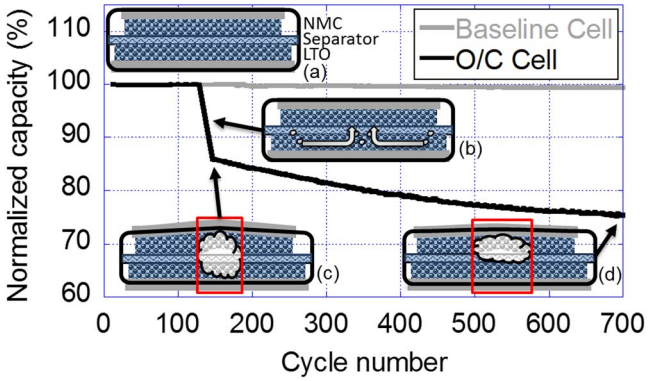

Figure 1. Capacity retention as a function of cycle number on the baseline cell (gray) and the O/C cell (black). Insets: schematic representation of the proposed gas evolution: (a) before, (b) during, (c) after and (d) long after overcharge. The blue tint represents the presence of liquid electrolyte, a cloud represents gas bubbles.

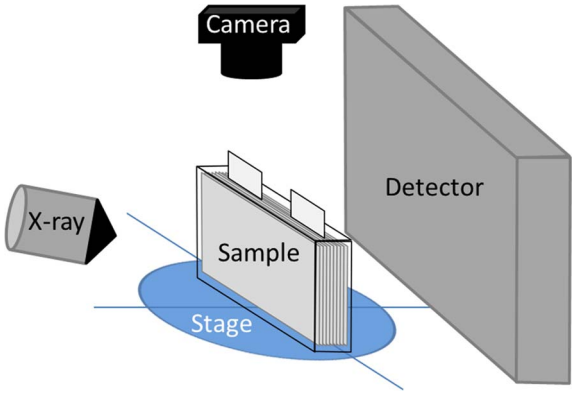

Figure 2. Experimental setup for the X-ray computerized tomography imaging of the O/C cell.

sizeable gas pocket, which spread over a large area between the two electrodes current collectors (Fig. 1c).

Regarding the second stage of degradation, the absence of LLI should be synonymous with no additional gas generation. However, the previously released gas would still be present. The intricate interaction of cycle-induced swelling/contracting within the electrodes and the gas volume distribution (with its associated pressure gradient) might act as the culprit for the propagation of the gas bubbles over a larger portion of the electrode stack. This would result into additional mechanical separation and ionic insulation of active materials in the electrode matrices and the stack, as pictured in Figure 1d where the same finite volume of the gas pocket as in Figure 1c spread over to a larger footprint as cycle aging continues. Again, the observation of a similar quantity of LAM at both PE and NE (8% LAM_{NE} and 8% LAM_{PE}) provided support to this hypothesis.

Experimental

Overcharge protocol.—Several commercial-grade LTO || NMC large-format pouch cells were acquired from a commercial manufacturer. Two of these cells, the O/C cell and the baseline cell, were subjected to the same cycle aging conditions, with and without the overcharge event respectively.[1] In order to validate the formulated hypothesis regarding the evolution and propagation of gas within the O/C cell, a third cell, the CT cell, has been used to replicate the overcharge event while monitoring gas evolution via CT scanning. The overcharge event was imposed to the CT and the O/C cells in an identical fashion: following a routine C/3 cycle aging to discharge the cell to 1.8 V, both cells were recharged using a CC-CV charging schedule (CC = C/4 to 3.6 V and CV = 3.6 V with a cutoff at C/25) to create the intended overcharge event. We imaged the CT cell using the CT scanning technology before and after imposing overcharge conditions.

Computerized tomography scanning (CT scan).—CT scan characterization is a non-destructive way to image the internal physical structure of a cell at varying depth. The CT scan technique is often used by battery manufacturers to ensure the proper alignment of electrode sheets and to detect the presence of internal defects within a cell. In battery studies, this technique is used to observe and assess the internal construction of the cell and any variations between test conditions or samples.[12,13] Our experiment was conducted on a Shimadzu SMX-225CT scanner using the following test settings: tube voltage set to 210 kV and tube current set to 130 μA. Additionally, we selected to operate in off-set mode because it offers the finest resolution for samples larger than 10 cm in width. Due to elevated power settings, the presence of filter became mandatory to protect the detector and we employed a 0.5 mm thick copper plate filter. Figure 2 presents a schematic example of the test setup for a pouch cell inside a CT scanner.

Using this setup, the image resolution was found to be sufficient to distinguish features of 300 μm or larger. Unfortunately, any feature that is smaller cannot be singled out and it is then difficult to distinguish the anode and cathode layers since their thickness is about 100 μm. Nonetheless, using this imaging technology, we sought to locate gas bubbles, 300 μm thick or more, within the electrode stack. The pouch cell was scanned from top to bottom over about 150 increments of depth progressing along the smaller dimension of the cell (i.e. its thickness). We also scanned the pouch cell from one end to the opposite end along the width. Scans with the most prominent features were selected for presentation. In the CT scans presented in this paper, a light colored area is indicative of the presence of matter, whereas a dark colored area is indicative of voids in the assembly.

Massage.—Upon confirmation of the presence of gas bubbles inside the stack by the CT scans, an attempt to displace existing gas bubbles was made. In order to do so, we performed a brief massage by hand with the O/C pouch cell lying flat on a table. Specifically, the pouch cell was rubbed from the center to the edges so that gas bubbles trapped within the core of electrode stack could be moved to the periphery and possibly escape the stack through its edges. Reference performance tests, identical to those described previously,[1] were carried immediately before and after the massage procedure to detect changes in the returned capacity and/or the thermodynamic configuration of the cell. As a precaution, the cell was fully charged before the massage because we were expecting to reconnect portions of electrodes in a state associated with the end of charge (capacity lost as a result of an overcharge). The decision to fully charge the cell was aimed at mitigating composition gradients within the cell's electrodes, which might have resulted in elevated internal currents. The voltage of the cell was monitored and recorded using a 22-bit USB Personal DAQ/56 data acquisition system from Measurement Computing. The sampling period was of 2 seconds for a total experiment duration of 5 minutes.

Results and Discussion

Electrochemical characterization of the overcharge event.—Figure 3a summarizes the voltage vs. capacity data collected during the overcharge and the subsequent discharge. It can be seen that during a regular charge to an end-of-charge (EOC) voltage of 2.8 V, approximately 15 Ah were returned to the cell. When the cell's voltage was increased to the 3.6 V end-of-over-charge (EOOC) voltage, and additional 2.4Ah were returned to the cell. At this point in time, the O/C cell started to exhibit a very noticeable swollen shape - typically indicative of gassing - which perdured until the time of the writing. In the

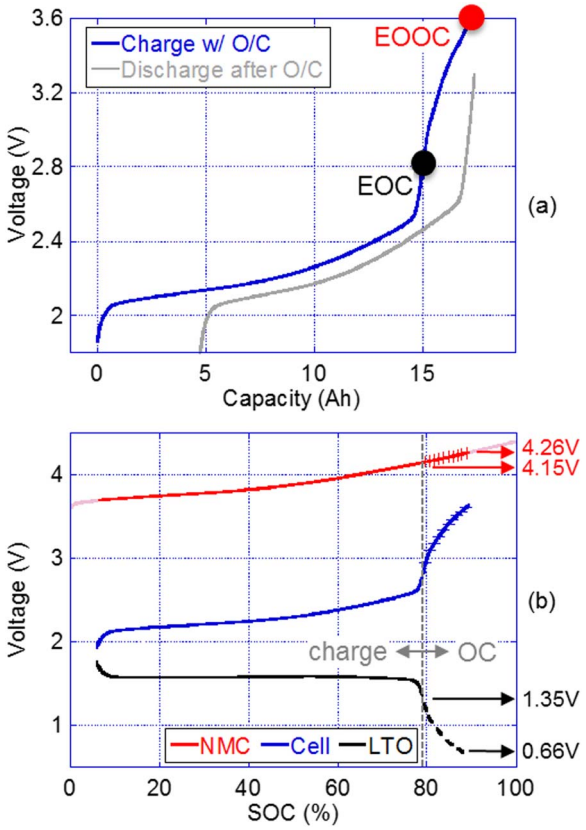

Figure 3. Representation of the 116% overcharge event. (a) Measured cell's voltage while overcharging (in blue) and during the subsequent discharge (in gray). Solid circles showcase the regular end-of-charge (EOC) cut-off voltage (in black) and the end-of-overcharge (EOOC) cut-off voltage (in red). (b) Cell's voltage and electrodes' potentials as modeled in the 'alawa toolbox. A solid line indicates the data were measured whereas a dashed line indicates the data were extrapolated. Crossbars highlight the excursion into overcharge. As-modeled end-of-charge and end-of-overcharge potentials of both electrodes are reported on the right Y-axis.

subsequent discharge, the O/C cell returned roughly 85% of the previously measured reversible capacity (i.e. 12.8 Ah), which implied that the additional 2.4Ah returned capacity were not reversible and even detrimental to the cell. Looking at the shape of the voltage response in details it can be seen that during the overcharge, the evolution of the voltage curve beyond 2.8 V seems oddly shaped in comparison to the voltage curve below 2.8 V. The curvature became convex above 2.8 V whereas it was mostly concave below 2.8 V. Investigating this voltage curve, in particular in its portion over 2.8 V might then reveal the impact of the overcharge with respect to each of the electrodes.

To investigate the behavior of each electrode individually under overcharge conditions, the main hurdle was to probe the electrode's potential. A commercial sealed pouch cell is not built with a third reference electrode and therefore, there is no direct potential sensing capability of individual electrode response. In order to circumvent this limitation, we estimated the individual electrode responses using the emulated cell model derived in part I of this work.[1] This model is the basis for our in-situ inference technique and consists of two datasets and two parameters. According to the 'alawa model[5,14] the reconstruction of a cell's voltage curve can be accomplished by composing the half-cell characteristics of PE and NE, as measured in ad-hoc experiments, and adjusting two parameters, the loading ratio (defined as the ratio of the specific area capacity in the NE versus that in the PE) and the initial offset (defined as the SOC slippage of the NE with respect to the SOC of the PE).

A visual representation of the emulation of a fresh commercial cell is presented in Fig. 3b. According to our simulations,[1] the loading ratio of a fresh cell is 77% and the offset 6%. A loading ratio lower than 1 implies that there is excess capacity in NMC at the end of charge. Specifically, we derived that upon completion of a regular 2.8 V charge, the potential at the surface of NMC is 4.15 V vs Li/Li^+ (all potentials thereafter are expressed versus Li/Li^+), and thus NMC is far from being fully delithiated. The corresponding potential at the surface of LTO is 1.35 V. We corroborated our findings with the help of a patent filed by the manufacturer.[15] Based on the information disclosed in this document the NMC and LTO electrodes do indeed reach surface potentials of 4.15 and 1.35 V at the end of charge, respectively.[15]

With the accuracy of the model in the [1.8 - 2.8 V] domain established, the cell's model introduced in Fig. 3b can be further used to estimate the LTO potential evolution during the 3.6 V overcharge. Indeed, although we did not have actual half-cell data of the LTO potential evolution in the [2.8 - 3.6 V] domain, we had measurement for the NMC half-cell up to 4.4 V. Consequently, the extrapolated LTO potential evolution could be composed by subtracting the cell's voltage from the NMC potential, as showcased in Fig. 3b in the OC domain where solid lines are an indication that NMC and full cell data were measured while a dashed line indicates that LTO data were inferred.

Based on this extrapolation, we estimated that when the O/C cell reached 3.6 V, NMC reached a potential of 4.26 V while LTO dropped to 0.66 V. A surface potential of LTO of 660 mV was not compatible with lithium plating conditions, but it could indicate that electrolyte reduction conditions (i.e. lower than 1 V) were present at the NE during overcharge. Moreover, the potential reached by the PE (i.e. 4.26 V) did not appear to be high enough to trigger electrolyte oxidation in any significant proportion. Indeed, this potential is comparable to the one a NMC electrode would reach during a typical usage of a graphite || NMC cell: when charged to 4.2 V, the actual surface potential of the NMC electrode tends to reach 4.28 V as a result of the graphite's 80 mV potential during the final stage of intercalation.[16] We therefore reached the conclusion that the NMC electrode did not overcharge during the 3.6 V overcharge imposed to the O/C and CT cells and that our investigation on the origin of the gassing should be focused on LTO.

With conditions for lithium plating and electrolyte oxidation ruled out, our focus could be narrowed further down towards possible electrolyte decomposition by reduction at the NE. To further investigate these reductive conditions, we differentiated the LTO's capacity with respect to the LTO's potential to yield the dQ/dV curve showcased in Fig. 4. The use of dQ/dV curves for analysis of electrolyte

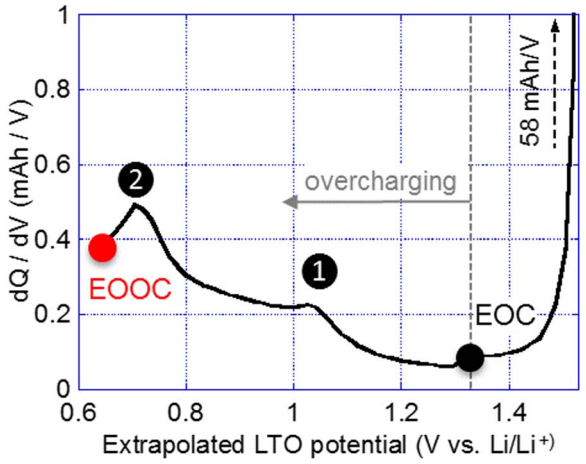

Figure 4. dQ/dV curve of the LTO electrode during overcharge obtained through differentiation of the extrapolated electrode's potential (see Fig. 3b). Two peaks in the IC curve are identified: ❶ around 1 V, ❷ around 0.7 V. Solid circles showcase the regular end-of-charge (EOC) cut-off potential (in black) and the end-of-overcharge (EOOC) cut-off potential (in red).

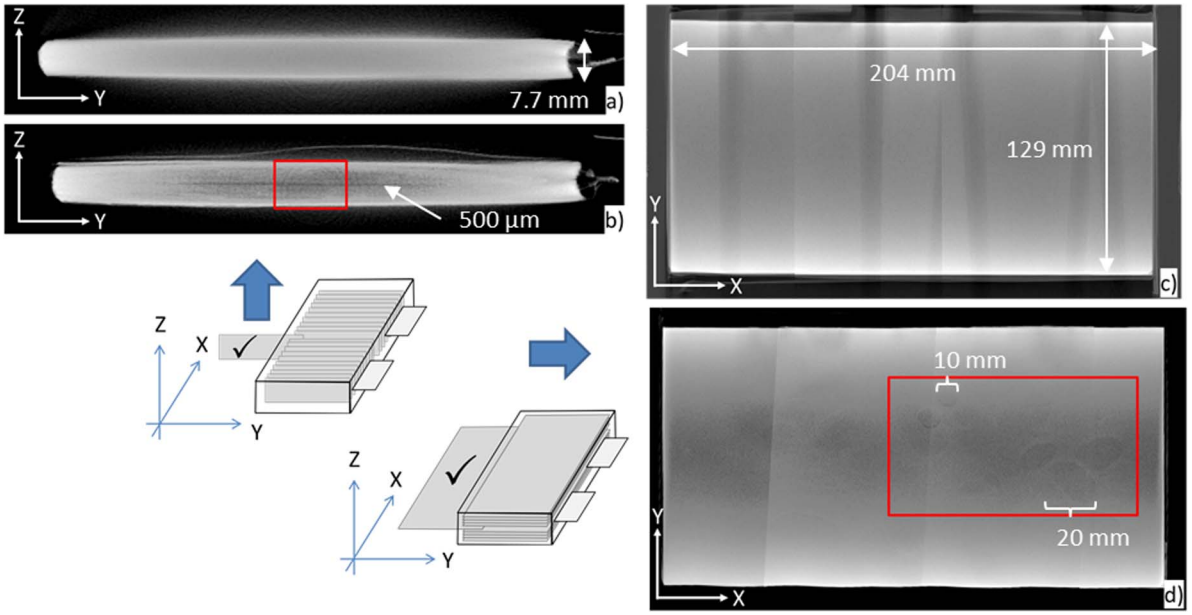

Figure 5. Tomograms of a pouch cell: before overcharge (a) in the Y-Z plane and (c) in the X-Y plane; after the overcharge (b) in the Y-Z plane and (d) in the X-Y plane. Remarkable features are highlighted using red rectangles. Matter colored in white, void colored in black. The largest bubbles are approximately 20 mm in diameter and the most visible gaps are 500 µm in thickness.

decomposition accompanying SEI formation has been successfully employed previously.[17–21] While a regular 2.8 V charge allowed the LTO potential to reach 1.35 V at its lowest, it was established that under the imposed overcharge conditions, the LTO potential evolved down to 0.66 V. The IC curve presented Fig. 4 showcases the presence of two peaks between the normal end-of-charge potential of 1.35 V and the end-of-overcharge at 0.66 V: ❶ around 1 V, ❷ around 0.7 V. The shapes and potentials associated with both peaks are reminiscent of the peaks observed by other researchers during known occurrences of carbonate solvent based electrolyte decomposition.[22–24]

From this electrochemical analysis, one can conclude that the overcharged LTO || NMC pouch cells encountered reductive conditions compatible with decomposition of carbonate solvent based electrolyte under the 3.6 V overcharge conditions. As a result of this electrolyte decomposition, generation of gaseous products is a likely outcome based on the available literature.[23–27]

Gas evolution (CT-scan experiment).—Visual indication of gassing (swollen pouch cell) as well as inferred indication of electrolyte decomposition at the interface between electrolyte and LTO prompted us to investigate the internal structure of the O/C cell to try to assess the spatial distribution of gas in the cell and understand how it affected the cell's capacity. A pristine cell, the CT cell, was devoted to this experiment. Before the overcharge, the CT cell offered a uniform white halo under CT scan imaging in both the Y-Z (Fig. 5a) and X-Y (Fig. 5c) planes and did not exhibit any visible gas bubble within the electrode stack. This was expected because, when not abused, these cells present a tightly packed appearance, indicative of an absence of gaseous byproducts. After the overcharge, a large volume of gas is visible in the region between the top of the stack and the soft bag (Fig. 5b). A white curve line is visible and corresponds to the edge of the top wall of the soft bag. Furthermore, a dark stripe, located at mid-depth, emerged in the Y-Z plane. At mid-depth, the presence of a number of moderate-size gas bubbles is evidenced by the CT scan in the X-Y plane.

The CT scan analysis showcased two areas where gasses seemed to accumulate: at the top and at mid-depth of the cell. So long as a sufficient volume of liquid electrolyte remained in the cell to wet the entirety of the electrodes, we do not expect the gas trapped at the top of the cell between the electrode stack and the soft bag to cause any capacity fade. On the contrary, it is our belief that the gas bubbles evidenced by voids at mid-depth in the electrode stack mechanically separated viable portions of the PE and NE from each other, disabling the ionic conduction pathway in the process. This ionic conduction pathway blockage would provide the basis for explaining the occurrence of LAM at both the PE and the NE. If this is true, then displacing these trapped gas bubbles away from the electrode stack and into the larger gas volume trapped under the top wall of the soft bag and permit the liquid electrolyte to wet the separator again should restore the ionic conduction pathway and allow these disabled areas to become active again, therefore regaining some of the lost capacity. In addition, breaking up the larger gas bubbles into tinier ones could help partially restore ionic conductivity as well.

Recovery massage.—To test this capacity recovery hypothesis, we administered a massage to the O/C cell. A recording of the instantaneous voltage across the O/C cell is displayed in Fig. 6. While rubbing the cell, the voltage across the cell was decreasing from approximately 2.62 V down to 2.54 V by the time the massage stopped. In particular, the voltage dropped rapidly within the first minute of the

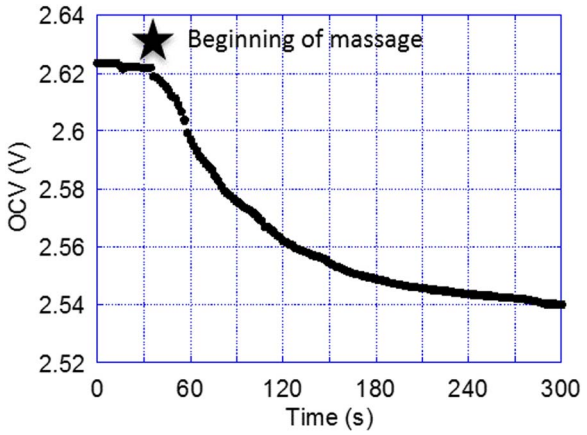

Figure 6. Open-circuit voltage of the O/C pouch cell while administering a massage by hand for 5 minutes. The massage began after 30 seconds.

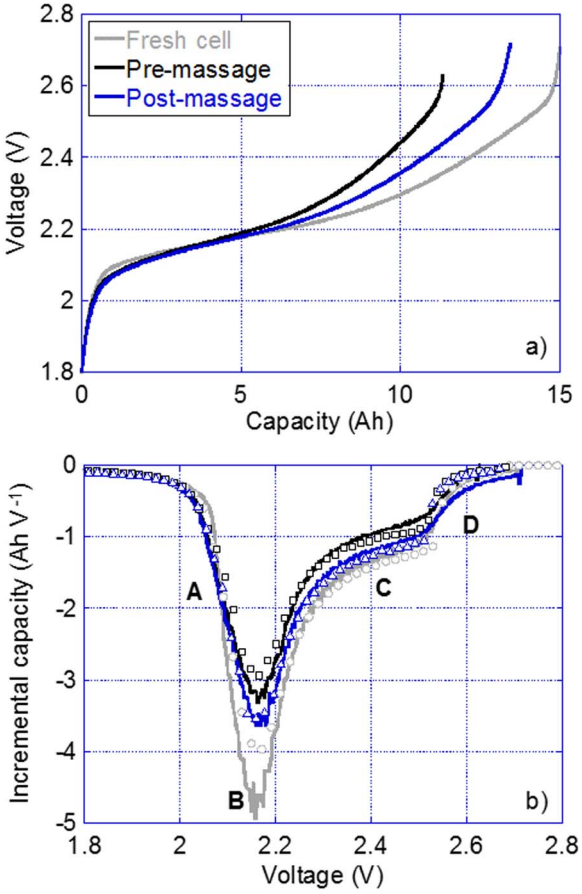

Figure 7. Consequences of the massage therapy on the O/C cell: (a) voltage curves during C/25 discharge as measured before overcharge (in gray), immediately before the massage (in black) and immediately after the massage (in blue); (b) dQ/dV curves before overcharge (in gray), immediately before the massage (in black) and immediately after the massage (in blue). Solid lines are indicative of experimental data while markers are indicative of 'alawa emulation data. ABCD markers are used to identify important features on these curves.[5]

rub. Thereafter, the evolution slowed down and after interrupting the massage, the voltage across the cell settled into a close-to-equilibrium state. There were two possible explanations for the observed voltage decrease. The first one is that while pressing the cell, local short-circuits were created that drove the cell's voltage down by slightly self-discharging the cell. Another way the cell's voltage could decrease in the observed fashion would be by connecting active material with a lower SOC to the existing active material. The respective SOCs would then equalize toward a weighted average quantity under the driving force of the concentration gradient and we would attain a rather stable lower OCV after some time. With the voltage settling down after a few minutes, we judged the short-circuit scenario less likely as it would continue to self-discharge the cell and favored the second "reconnection" scenario. To make sure, we submitted the post-massage O/C cell to a reference performance testto figure out whether or not the capacity of the cell had changed and whether or not the thermodynamic balance of the cell had been modified owing to the massage.

Figure 7a presents the C/25 voltage vs. capacity characteristics of the O/C cell in the fresh state (in gray) as well as before (in black) and after (in blue) the administered massage. By the time the massage was administered, the O/C had been cycled for 1500 cycles and presented an overall capacity loss of 25%, to be compared to the 23% after 700 cycles reported in our previous communication. As expected, the massage allowed to recover some capacity and after the massage, the cell returned 13.45 Ah as opposed to 11.35 Ah before. However, it did not recover its initial capacity (15.0 Ah). The capacity recovered by massage was on the order of 18.6% of the capacity before the massage or 14% of the capacity of a fresh cell. For the sake of consistency, for the remainder of this discussion, all quantities will be expressed on a scale based on a fresh cell. In order to verify that the significant capacity recovery was induced by the reconnection of portions of NMC and LTO electrodes disabled by the presence of gas bubbles, we performed a dQ/dV analysis[1,5] on the C/25 data recorded, Figure 7b. To facilitate the discussion, the ABCD markers from the first part of this work[1] have been re-used. First, the region 'A' did not move as a result of the massage, which tends to indicate that the offset was not affected by the massage and its associated reconnection of AM. Second, the intensity of the regions 'B' and 'C', associated with the amount of PEAM, increased significantly. This is a direct indication that more PEAM is being utilized inside the cell, thus reflecting an increase of accessible PEAM owing to the administered massage. Finally, the position of the region 'D' did not move much as identified by the fact that the transition from shoulder to tail occurred at more or less the same cell's voltage. In the previous part, we established that the locations of the regions 'A' and 'D' are very sensitive to the loading ratio of the cell.[1] The fact that both 'A' and 'D' markers maintained their positions suggests that the relative amounts of PEAM and NEAM (i.e. the loading ratio) remained the same through massaging. Since it was unambiguously determined that more PEAM is involved in the reaction (i.e. regions 'B' and 'C'), the only way that the loading ratio would have remained constant is that similar amounts of NEAM have been reactivated as well. In fact, this appears to be the reverse process of how the capacity had been lost in the first place - reactivation vs. deactivation of AM in similar proportions from NE and PE.

Analysis of the capacity recovery.—What proportions of NEAM and PEAM were recovered precisely because of this massage can be investigated with help of the model of the cell represented in Figure 3b. Indeed, it can be established that the capacity of the cell in the [1.8–2.8] V range is strictly equal to the capacity of the NE by virtue of the NE being the limiting electrode at both end-of-charge and end-of-discharge. As a result, the fact that the massaged cell recovered 14% of its initial capacity was a trivial indication that the 14% of the entire NEAM had been reconnected. And because we established earlier that the loading ratio remained constant throughout the massage, we concluded that 14% of the entire PEAM were recovered at the same time. This 14% recovery was corroborated by a similar increase in the average intensity of the marker 'C', which we previously identified to be a direct probe of the total quantity of PEAM. Overall, we estimated that 14 of the 25% of the lost AM had been recovered because of the massage. That means that we were seemingly able to reconnect 55% of the disconnected AM through massage.

We then tried to take this analysis one step further by providing an estimate of the lithiation state of both PEAM and NEAM as they were recovered. That is, we sought to quantify what proportion of the recovered PEAM was lithiated and what proportion of the recovered NEAM was delithiated. In essence, the recovered AM was a combination of gain of active material (GAM) from both electrode in each lithiation state: GAM_{dePE}, GAM_{liPE}, GAM_{deNE} and GAM_{liNE}. In the paragraphs below, it is important not to confuse SOC quantities with AM quantities, which are different normalized quantities. The percentage of AM is normalized to the initial quantity of AM in the fresh cell. The SOC is normalized to the available amount of active of AM and will be comprised between 100% and 0% at any stage of the life of the cell. To help distinguish between them and avoid any possible confusion, we represented SOC quantities as percentages of SOC ($\%_{SOC}$) and we represented quantities of AM as percentage of AM ($\%_{AM}$).

Figure 8 shows the recovery scheme for PEAM with stacked vertical bars that represent the distribution of the states of PEAM as delithiated, lithiated and inactive (i.e. LAM). The objective of the analysis to follow is to estimate these three quantities both pre- and post-massage and use that knowledge to deduct the state of the recovered portion of PEAM (i.e. GAM).

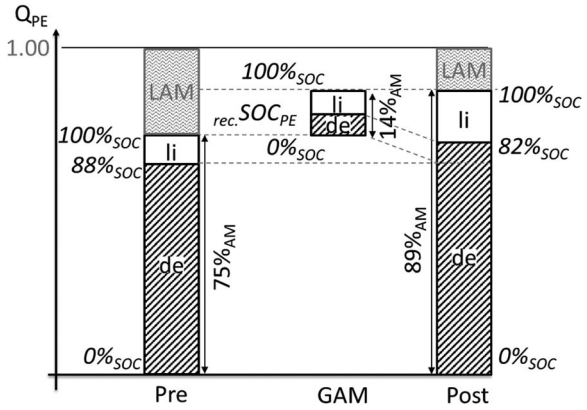

Figure 8. A stacked columns representation of the evolution of the positive electrode active material pre- (left), during (GAM, center) and post-massage (right). "LAM" stands for Lost Active Material, "li" for lithiated state, "de" for delithiated state and GAM for Gained Active Material.

We begin with quantifying the overall amount of PEAM recovered because of the massage with respect to the initial PEAM quantity (i.e. $100\%_{AM}$). In the section above, we estimated that the recovery of PEAM amounted to $14\%_{AM}$. That is:

$$_{recovered}Q_{PE} = \text{GAM}_{PE} = \text{GAM}_{\text{liPE}} + \text{GAM}_{\text{dePE}} = 14\%_{AM} \quad [1]$$

It can further be established that the proportions of lithiated and delithiated AM recovered at the PE are proportional to the SOC of the recovered AM. Indeed, as the SOC is normalized on the available AM, the lithiation state is directly proportional to the SOC. For GAM in Figure 8, it results that:

$$GAM_{dePE} = GAM_{PE} * {}_{recovered}SOC_{PE} \quad [2]$$

$$GAM_{liPE} = GAM_{PE} * (100 - {}_{recovered}SOC_{PE}) \quad [3]$$

Where $_{recovered}SOC_{PE}$ refers to the SOC of the recovered AM alone. This $_{recovered}SOC_{PE}$ is therefore the parameter we need to calculate to be able to approximate the lithiation state of the GAM_{PE}.

With the help of Figure 8, we can establish that the $_{recovered}SOC_{PE}$ can be expressed from the SOCs of the PEAM pre- and post- recovery, $_{pre}SOC_{PE}$ and $_{post}SOC_{PE}$ respectively. To visualize this relationship we can use an analogy and look at the 3 vertical stacked bars as liquid columns of the same diameter. In this analogy, the delithiated PEAM corresponds to the volume of liquid and the SOC to the percentage of filling relative the height of the column. Using this analogy, the gain of active material can be seen as the transfer of the liquid from the Pre and the GAM columns into a Post column, whose height is the sum of the height of the Pre and GAM column. The volume of liquid in the Post column will then be equal to the volume of liquid in the Pre column plus the volume of liquid in the GAM column. Since all columns have the same diameter, the volume is directly proportional to the percentage of filling times the height of the column. From this analogy, a weighted average relationship between the different SOCs and their respective amounts of active material that can be deciphered:

$$_{post}SOC_{PE} * {}_{post}Q_{PE} = {}_{recovered}SOC_{PE} * {}_{recovered}Q_{PE} + {}_{pre}SOC_{PE} * {}_{pre}Q_{PE} \quad [4]$$

Which can be rewritten as:

$$_{recovered}SOC_{PE} = \left({}_{post}SOC_{PE} * {}_{post}Q_{PE} - {}_{pre}SOC_{PE} * {}_{pre}Q_{PE}\right) {}_{recovered}Q_{PE} \quad [5]$$

At this stage, we are looking at Equation 5 where the quantities of PEAM are known (i.e. $_{post}Q_{PE} = 89\%_{AM}$, $_{pre}Q_{PE} = 75\%_{AM}$ and $_{recovered}Q_{PE} = 14\%_{AM}$) but where all three SOCs are unknown. Therefore, to solve this equation, we need to estimate $_{pre}SOC_{PE}$ and $_{post}SOC_{PE}$. With the help of the model developed for the full cell in the first part of this study,[1] we can relate the OCV measured across the full cell before and after recovery (see. Fig. 6) to the SOC of the PE, which will allow us to estimate the SOCs. Indeed, at end-of-charge, we expect the NE to be at the very end of its potential plateau at equilibrium and therefore present a fairly constant 1.58 V potential. By subtracting these constant 1.58 V from the measured OCV (i.e. 2.62 V pre-recovery and 2.54 V post-recovery), we could obtain a rough estimate of the potential of the PE at equilibrium and therefore estimate the SOC of the PE using the $SOC = f(OCV)$ characteristic collected for this NMC-based PE. That is:

$$_{post}SOC_{PE} = f_{SOC}\left({}_{post}OCV - {}_{plateau}V_{NE}\right) \quad [6]$$

$$_{pre}SOC_{PE} = f_{SOC}\left({}_{pre}OCV - {}_{plateau}V_{NE}\right) \quad [7]$$

Where $_{pre}OCV = 2.62\ V$, $_{post}OCV = 2.54\ V$ and $_{plateau}V_{NE} = 1.58\ V$.

Using Equations 6 and 7 it was found that the SOCs of the PE were $88\%_{\text{SOC}}$ and $82\%_{\text{SOC}}$ pre-recovery and post-recovery, respectively. As a result, $_{recovered}SOC_{PE}$ must have been around $50\%_{\text{SOC}}$ according to Equation 5. Using Equation 2 and 3, we can now estimate GAM_{dePE} and GAM_{liPE} to be $7\%_{AM}$.

Following this investigation of the lithiation of the PEAM, the next step is to investigate the recovered NEAM. Since we already estimated that the recovery of NEAM amounted to $14\%_{AM}$, we can first establish that:

$$_{recovered}Q_{NE} = \text{GAM}_{NE} = \text{GAM}_{\text{liNE}} + \text{GAM}_{\text{deNE}} = 14\%_{AM} \quad [8]$$

Also, since we previously observed that the offset was largely unaffected by the recovery, as indicated by a stationary 'A' marker, we can use this information to estimate GAM_{liNE}. Indeed, we showed in a prior study that the offset is affected by the sole evolution of two quantities, the loss or gain of delithiated PEAM and/or the loss or gain of lithiated NEAM.[5] This relationship can be transcribed as:

$$\Delta OFS = 0\% \Leftrightarrow GAM_{dePE} - LR * GAM_{liNE} = 0 \quad [9]$$

Where ΔOFS is the variation of the offset because of the recovery (i.e. null) and LR is the loading ratio at the time of the recovery (i.e. 0.77).

Because GAM_{dePE} had been evaluated earlier (i.e. $7\%_{AM}$), we were able to solve Equation 9 for GAM_{liNE} and found it to be $9.1\%_{AM}$. Finally, using Equation 8, we can estimate GAM_{deNE} to be $4.9\%_{AM}$. This serves as an indication that the SOC of the recovered NEAM was around 65% (i.e. predominantly lithiated).

We sought confirmation of these findings by emulating the cell using the 'alawa degradation diagnosis toolbox after the massage.[14] GAM were emulated by inputting negative quantities in the relevant LAM parametric fields (i.e. representing a gain as a negatively signed loss). The result of this emulation can be found in Figure 7b where the experimental data are represented as solid lines while the emulated data are represented as markers. The fit between emulation and experimental post-recovery (in blue) is satisfactory with the notable exception of the tail region beyond 'D' (i.e. above 2.5 V) where the experimental curve lies higher than the emulated curve. Based on our emulation, the tail should quickly return to a near-zero intensity because pristine LTO has little electrochemical activity in the potential range below 1.35 V. We estimated that this extra capacity at high voltage accounted for less than 16% of the recovered capacity. At the time of writing, the origin of this increased electrochemical activity at low potential on the NE (i.e. high cell voltage) could not be explained.

Conclusions

In this paper, we validated the hypothesis we proposed initially regarding how a LTO || NMC pouch cell having sustained an overcharge had been losing capacity through the generation and entrapment of gas bubbles within the electrode stack. First, using a dQ/dV analysis, we

identified the transient reductive conditions, which in the context of a LTO-based cell resulted into substantial electrolyte decomposition. Second, we used a CT scanner to image the internal structure of a cell before and after overcharge and obtained evidence of the presence of gas bubbles trapped between PE and NE within the electrode stack. The physical separation of both electrodes created by these gas bubbles appeared large enough to disrupt the ionic conduction pathway, therefore disabling portions of otherwise perfectly viable electrodes. This was later demonstrated by administrating a massage to the O/C cell in an effort to displace the trapped gas bubbles outside of the electrode stack. The massage helped reconnecting 14 of the 25% of the lost active materials and restore nearly 60% of the capacity lost to the overcharge and its aftermath. Ultimately, this study illustrates the durability of this LTO || NMC cell design against overcharge. It also showcases the detrimental effect of electrolyte-reduction-induced gassing with LTO electrodes allowed to discharge below 1 V and explains the mechanism through which the overcharge drove the capacity to fade.

Acknowledgments

Authors would like to acknowledge the concourse of the Underwriters' Laboratory (UL) of Taiwan in producing CT-scans of the pouch cell.

This work was funded by ONR Hawaii Energy and Environmental Technologies (HEET) 2010 Initiative, award No N00014-11-1-0391.

The authors would like to thank Jerry Haverstick, Len Sekowski and Mike Coleman (Altairnano) for their help throughout the course of this study.

References

1. A. Devie, M. Dubarry, and B. Y. Liaw, *J. Electrochem. Soc.*, **162**, A1033 (2015).
2. M. Dubarry and B. Y. Liaw, *J. Power Sources*, **194**, 541 (2009).
3. M. Dubarry, C. Truchot, M. Cugnet, B. Y. Liaw, K. Gering, S. Sazhin, D. Jamison, and C. Michelbacher, *J. Power Sources*, **196**, 10328 (2011).
4. M. Dubarry, C. Truchot, B. Y. Liaw, K. Gering, S. Sazhin, D. Jamison, and C. Michelbacher, *J. Power Sources*, **196**, 10336 (2011).
5. M. Dubarry, C. Truchot, and B. Y. Liaw, *J. Power Sources*, **219**, 204 (2012).
6. I. Belharouak, G. M. K. Jr., and K. Amine, *J. Power Sources*, **196**, 10344 (2011).
7. I. Belharouak, G. M. Koenig, T. Tan, H. Yumoto, N. Ota, and K. Amine, *J. Electrochem. Soc.*, **159**, A1165 (2012).
8. Y.-B. He, B. Li, M. Liu, C. Zhang, W. Lv, C. Yang, J. Li, H. Du, B. Zhang, Q.-H. Yang, J.-K. Kim, and F. Kang, *Sci. Rep.*, **2**, 913 (2012).
9. R. Bernhard, S. Meini, and H. A. Gasteiger, *J. Electrochem. Soc.*, **161**, A497 (2014).
10. L. G. Butler, E. H. Lehmann, and B. Schillinger, *Physics Procedia*, **43**, 331 (2013).
11. J. B. Robinson, J. A. Darr, D. S. Eastwood, G. Hinds, P. D. Lee, P. R. Shearing, O. O. Taiwo, and D. J. Brett, *J. Power Sources*, **252**, 51 (2014).
12. M. J. Brand, S. F. Schuster, T. Bach, E. Fleder, M. Stelz, S. Glaser, J. Muller, G. Sextl, and A. Jossen, *J. Power Sources*, **288**, 62 (2015).
13. V. Yufit, P. Shearing, R. Hamilton, P. Lee, M. Wu, and N. Brandon, *Electrochem. Commun.*, **13**, 608 (2011).
14. 'alawa central, Website, https://www.soest.hawaii.edu/HNEI/alawa.
15. V. Manev, Methods for improving lithium ion battery safety, https://www.google.com/patents/US20090017364 (2009).
16. T. Ohzuku, Y. Iwakoshi, and K. Sawa, *J. Electrochem. Soc.*, **140**, 2490 (1993).
17. E. Peled, D. Golodnitsky, C. Menachem, and D. Bar-Tow, *J. Electrochem. Soc.*, **145**, 3482 (1998).
18. D. Abraham, M. Furczon, S.-H. Kang, D. Dees, and A. Jansen, *J. Power Sources*, **180**, 612 (2008).
19. L. El Ouatani, R. Dedryvere, C. Siret, P. Biensan, and D. Gonbeau, *J. Electrochem. Soc.*, **156**, A468 (2009).
20. J. C. Burns, R. Petibon, K. J. Nelson, N. N. Sinha, A. Kassam, B. M. Way, and J. R. Dahn, *J. Electrochem. Soc.*, **160**, A1668 (2013).
21. R. Petibon, E. C. Henry, J. C. Burns, N. N. Sinha, and J. R. Dahn, *J. Electrochem. Soc.*, **161**, A66 (2014).
22. P. Arora, R. E. White, and M. Doyle, *J. Electrochem. Soc.*, **145**, 3647 (1998).
23. S.-D. Xu, Q.-C. Zhuang, J. Wang, Y.-Q. Xu, and Y.-B. Zhu, *Int. J. Electrochem. Sci*, **8**, 8058 (2013).
24. H. Kim, S. Grugeon, G. Gachot, M. Armand, L. Sannier, and S. Laruelle, *Electrochim. Acta*, **136**, 157 (2014).
25. K. Wu, J. Yang, Y. Liu, Y. Zhang, C. Wang, J. Xu, F. Ning, and D. Wang, *J. Power Sources*, **237**, 285 (2013).
26. L. Chancelier, A. Benayad, T. Gutel, S. Mailley, and C. C. Santini, *J. Electrochem. Soc.*, **162**, A1008 (2015).
27. T. Ohsaki, T. Kishi, T. Kuboki, N. Takami, N. Shimura, Y. Sato, M. Sekino, and A. Satoh, *J. Power Sources*, **146**, 97 (2005).